Communication

Halo-like Scaling from Rotational Stresses in Relativistic Matter

Piotr Ogonowski *

Posted Date: 9 May 2026

doi: 10.20944/preprints202603.1718.v2

Keywords: dark matter; MOND; galaxy rotation curves; Tully-Fisher relation; anisotropic stress; Alena tensor

 doi:10.20944/preprints202603.1718.v2

Communication

Halo-like Scaling from Rotational Stresses in Relativistic Matter

Piotr Ogonowski

Kozminski University, Jagiellonska 57/59, 03-301 Warsaw, Poland; piotrogonowski@kozminski.edu.pl

Abstract

A relativistic stress-energy configuration is identified in which halo-like scaling in galaxies can arise from the rotational sector of matter without modifying the Einstein equations. In stationary axisymmetric systems, the mixed stress-energy components associated with vorticity define a conserved Killing current describing angular-momentum transport. The corresponding stream potential admits a multipole structure in which the dominant odd mode controls the radial flux and fixes its asymptotic amplitude. If this transport channel approaches a finite large-radius flux, the leading mode scales as r^{-2}. With the Alena Tensor closure, the same rotational sector that carries this transport mode contributes to the active weak-field source through the rotational part of the stress-energy tensor, giving an effective density with the same radial scaling and therefore approximately flat rotation curves. The baryonic Tully-Fisher relation is treated here as a constraint on the asymptotic transport amplitude, not as a first-principles derivation. The resulting framework gives testable predictions for disk-aligned lensing anisotropy, residual correlations with baryonic angular momentum, and suppressed halo-like scaling in systems without coherent rotation.

Keywords: dark matter; MOND; galaxy rotation curves; Tully-Fisher relation; anisotropic stress; Alena tensor

1. Introduction

Galaxy rotation curves exhibit a well-known asymptotic behaviour: the circular velocity tends to approach a constant value at large radii, and the asymptotic velocity obeys the baryonic Tully-Fisher relation [1,2] $v_f^4 \propto GM_b a_0$, where M_b is the baryonic mass. These observations are typically interpreted either in terms of dark matter halos or in terms of modified low-acceleration dynamics [3,4]. An alternative possibility is that the observed phenomenology emerges from additional dynamical structure within the matter energy-momentum tensor itself, without introducing new particle species or modifying the Einstein field equations. Related approaches have explored the role of non-trivial energy-momentum exchange and effective dark sector behaviour within the stress-energy tensor itself [5]. In contrast to such scenarios, the mechanism proposed here attributes the effect specifically to the rotational sector of the matter energy-momentum tensor and the associated angular-momentum transport. Although derived within the Alena Tensor framework [6], the discussed mechanism relies only on the existence of non-vanishing mixed stress-energy components $T^r{}_\phi$ associated with angular-momentum transport thus similar structures are expected in any relativistic description of rotating matter with anisotropic stresses. The key observation is that rotational stresses contribute to the effective gravitating energy density of matter through the vorticity invariant. In the weak-field regime this contribution produces a halo-like density profile that leads to flat rotation curves and MOND-like scaling [7], similar in spirit to mechanisms where halo phenomenology emerges from additional stress-energy components rather than new particle species [8].

 doi:10.20944/preprints202603.1718.v2

2. Rotational Stresses and Asymptotic Halo

The Alena Tensor framework can be viewed as an effective relativistic fluid description with intrinsic coupling between shear and vorticity, leading to additional anisotropic stress components. In this construction the effective matter energy-momentum tensor derived from the Lagrangian density introduced in [6] can be written schematically as

$$T_{\mu\nu} = \rho U_\mu U_\nu - \Xi_{\mu\nu}, \quad \nabla^\mu T_{\mu\nu} = 0, \tag{1}$$

where $\Xi_{\mu\nu}$ encodes energy flux and rotational stresses associated with the vorticity of the flow. In this approach the system has a built-in anisotropic stress, but its source is not viscosity, but the coupling between shear and vorticity (between flow deformation and local spin angular momentum). The gravitational field in this framework satisfies the standard Einstein equations $G_{\mu\nu} + \Lambda g_{\mu\nu} = \kappa T_{\mu\nu}$, while the new effect arises from the rotational sector of the matter stress-energy tensor.

The explicit form of the effective stress-energy tensor obtained in the Alena Tensor framework can be written as

$$T_{\mu\nu} = \frac{\varepsilon}{c^2} U_\mu U_\nu + \frac{1}{c^2}(U_\mu q_\nu + U_\nu q_\mu) - E_{\rm rot}\, \Delta_{\mu\nu} - \tau_{\mu\nu}, \tag{2}$$

where U^μ is the four-velocity of the flow, q^μ denotes the energy flux, $\tau_{\mu\nu}$ is the anisotropic stress tensor, $\Delta_{\mu\nu} = g_{\mu\nu} - U_\mu U_\nu / c^2$ is the spatial projector orthogonal to the flow and the rotational energy density is proportional to the vorticity invariant $E_{\rm rot} \propto \omega_{\mu\nu}\omega^{\mu\nu}$, with $\omega_{\mu\nu}$ being the projected vorticity tensor.

The "halo" was already interpreted in [6] not as additional mass, but as a result of angular momentum transport via the energy flux q^μ and anisotropic stresses $\tau^\mu{}_\nu$, which generate non-zero fluxes $T^r{}_\phi$ and/or $T^\theta{}_\phi$. Recent results obtained within this framework actually show improved agreement with rotation curve data. Figure 1 provides a synthetic summary of the Alena Tensor (AT) vs. MOND rotation curves based on the appendix with data from [6].

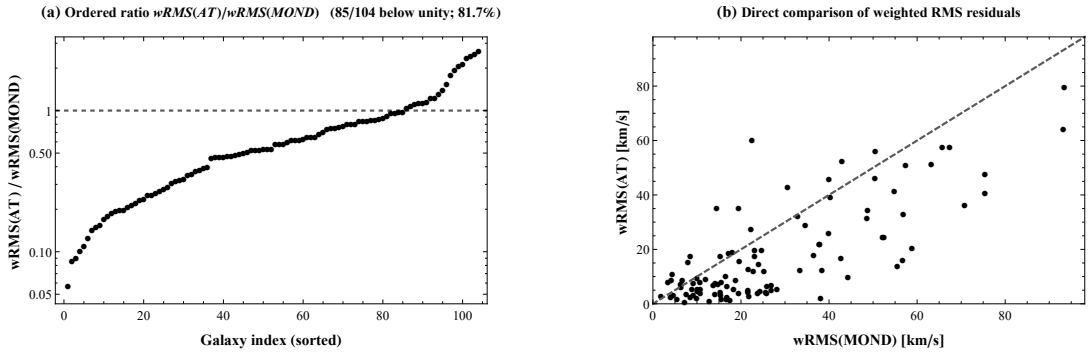

Figure 1. Comparison of weighted RMS residuals for the Alena Tensor benchmark and MOND for the 104-galaxy sample. Panel (a) shows the ordered ratio $wRMS(\mathrm{AT})/wRMS(\mathrm{MOND})$; 85 out of 104 galaxies lie below unity, corresponding to 81.7% of the sample. Panel (b) shows the direct comparison between $wRMS(\mathrm{AT})$ and $wRMS(\mathrm{MOND})$ in $\mathrm{km\,s^{-1}}$; the dashed line denotes equality. Points below the dashed line correspond to galaxies for which the AT benchmark gives a smaller weighted RMS residual than MOND.

However, the results obtained using the Alena Tensor can be considered as an example of a more general mechanism. For stationary axisymmetric systems the spacetime admits the rotational Killing vector $\xi^\mu_{(\phi)} = \partial_\phi$. The corresponding Killing current is

$$J^\mu_{(L)} = T^\mu{}_\phi. \tag{3}$$

Because $\nabla_\mu T^{\mu\nu} = 0$, the Killing current is automatically conserved

$$\nabla_\mu J^\mu_{(L)} = 0. \tag{4}$$

 doi:10.20944/preprints202603.1718.v2

In rotating astrophysical systems angular momentum transport is known to arise from correlated stresses and torques in the disk, suggesting that a quasi-stationary transport channel may naturally develop on galactic timescales. In axisymmetric coordinates this conservation law reduces to

$$\partial_r(\sqrt{-g}F_r) + \partial_\theta(\sqrt{-g}F_\theta) = 0, \tag{5}$$

where the flux components are

$$F_r = \frac{q^r U_\phi}{c^2} - \tau^r{}_\phi, \quad F_\theta = \frac{q^\theta U_\phi}{c^2} - \tau^\theta{}_\phi. \tag{6}$$

This equation has the structure of a two-dimensional continuity equation and therefore admits a stream potential $\Psi(r,\theta)$ defined by

$$\sqrt{-g}F_r = \partial_\theta \Psi, \quad \sqrt{-g}F_\theta = -\partial_r \Psi. \tag{7}$$

The angular structure of Ψ can be expanded in Legendre modes

$$\Psi(r,\theta) = \sum_\ell R_\ell(r) P_\ell(\cos\theta). \tag{8}$$

On the galactic plane ($\theta = \pi/2$) only odd multipoles contribute to the radial flux because $P'_{2m}(0) = 0$. The lowest non-vanishing contribution therefore corresponds to $\ell = 1$

$$\Psi(r,\theta) \approx R_1(r)\cos\theta. \tag{9}$$

By analogy with standard multipole expansions in long-range fields, higher-order modes are expected to decay faster with radius [9,10], so that the asymptotic behaviour is dominated by the lowest non-vanishing odd multipole $\ell = 1$. In the weak-field regime the metric determinant behaves asymptotically as $\sqrt{-g} \sim r^2$, which implies

$$F_r \sim \frac{R_1(r)}{r^2}. \tag{10}$$

If $R_1(r)$ approaches a constant value at large radii, the resulting transport flux scales as r^{-2}. The conversion of this transport scaling into a weak-field gravitational source is the role of the Alena Tensor stress-energy closure and is made explicit below.

3. Weak-Field Source and Post-Newtonian Ordering

A possible ambiguity concerns the distinction between the direct gravitomagnetic field of a rotating disk and the active weak-field source generated by the rotational stress sector. The mechanism discussed here does not identify the observed radial acceleration with the ordinary Lense-Thirring field of T^{0i} or with a purely kinematic frame-dragging correction. Such terms are post-Newtonian and are suppressed in galactic disks by powers of v/c.

The relevant source is instead the scalar active part of the stress-energy tensor entering the weak-field limit of the Einstein equations. With the conventions of Eq. (2), the rotational contribution to the effective gravitating density may be written schematically as

$$\rho_{\rm eff} = \frac{1}{c^2}\left(T^{\rm rot}_{00} + T^i{}_{i\,{\rm rot}}\right), \tag{11}$$

up to the usual sign conventions associated with the metric signature and spatial trace. Thus the radial acceleration is sourced by the rotational contribution to $T_{00} + T^i{}_i$, not by the gravitomagnetic field alone. In the Alena Tensor construction this source is not introduced as a post-Newtonian frame-dragging correction. It is the rotational part of the matter stress-energy tensor, containing the rotational energy density $E_{\rm rot}$, the energy flux q^μ, and the anisotropic stress $\tau_{\mu\nu}$ already present in Eq. (2). The

 doi:10.20944/preprints202603.1718.v2

mixed components $T^r{}_\phi$ and $T^\theta{}_\phi$ identify the angular-momentum transport channel, while the scalar weak-field source is supplied by the corresponding rotational contribution to $T_{00} + T^i{}_i$.

The non-trivial step is therefore not the existence of the transport current, but its scalar weak-field projection through the Alena Tensor stress-energy closure. In the stationary large-radius regime this closure is expressed by the proportionality

$$\rho_{\rm eff}(r, \pi/2) \propto \frac{F_r(r, \pi/2)}{c^2}, \tag{12}$$

where the proportionality is fixed by the stress-energy closure of the Alena Tensor theory and by the decomposition of the rotational sector into $E_{\rm rot}$, q^μ, and $\tau_{\mu\nu}$ in Eq. (2). Using Eq. (10), this gives

$$\rho_{\rm eff}(r, \pi/2) \propto \frac{R_1(r)}{r^2}. \tag{13}$$

Equations (12) and (13) are the bridge between the conserved transport current and the Newtonian source term. Without this closure, Eq. (10) would describe angular-momentum transport only and would not by itself constitute a gravitational halo. With the Alena Tensor closure, the same rotational sector that carries the angular-momentum flux also contributes to the active source defined in Eq. (11).

4. MOND-like Scaling, RAR and BTFR

The observational scaling relations place additional constraints on the allowed class of solutions. Galaxy rotation curves satisfy the radial acceleration relation (RAR) [11], which implies that the halo contribution must become negligible in the high-acceleration inner region while dominating at large radii. This requires that the radial function satisfies

$$R_1(r) = o(r^2) \quad (r \to 0), \tag{14}$$

so that the rotational sector does not affect the central baryon-dominated region.

A useful physical interpretation of the coefficient $R_1(r)$ follows from the conserved Killing current associated with rotational symmetry. The total radial flux of angular momentum through a sphere of radius r is given by

$$\dot{J}(r) = \int J^r_{(L)}\, dS = 2\pi \int_0^\pi d\theta\, \sqrt{-g}\, F_r. \tag{15}$$

Using the stream-potential representation

$$\sqrt{-g} F_r = \partial_\theta \Psi, \tag{16}$$

one obtains

$$\dot{J}(r) = 2\pi \int_0^\pi d\theta\, \partial_\theta \Psi = 2\pi[\Psi(r, \pi) - \Psi(r, 0)]. \tag{17}$$

For the dominant odd multipole (9) this yields

$$\dot{J}(r) = -4\pi R_1(r). \tag{18}$$

The coefficient $R_1(r)$ therefore has the direct physical meaning of the radial angular-momentum current carried by the rotational sector of the stress-energy tensor. In particular, the asymptotic amplitude is related to the asymptotic transport rate

$$R_\infty = -\frac{\dot{J}_\infty}{4\pi}. \tag{19}$$

The above assumption should be viewed not as a special choice but as the asymptotic fixed point of sustained angular-momentum transport. In a quasi-stationary regime, conservation of the Killing current implies that the total angular-momentum flux through spherical shells becomes approximately radius-independent at sufficiently large distances, unless balanced by external sinks or sources. Such

 doi:10.20944/preprints202603.1718.v2

quasi-stationary transport regimes, characterized by long-range angular-momentum redistribution and approximately constant fluxes, are well known in rotating astrophysical systems [12–15].

In the underlying Alena Tensor framework, the radial mode $R_1(r)$ is not a fundamental degree of freedom but the leading odd multipole of the stream potential associated with the conserved angular-momentum Killing current. Its dynamics is thus induced by the rotational sector of the stress-energy tensor, through the energy flux q^μ and anisotropic stress $\tau_{\mu\nu}$, which are generated by the vorticity, shear, and acceleration of the flow. In a fully dynamical treatment, $R_1(r)$ would therefore be determined by the coupled evolution of these quantities together with the spacetime geometry. In the present Letter, the full transport problem is not addressed explicitly. Instead, the focus is placed on the asymptotic regime, in which the radial angular-momentum current approaches, as expected from the conservation argument above, a finite value at large radii. This allows one to isolate the generic consequences of rotational stresses for the large-scale gravitational field.

At large radii the asymptotic behaviour $R_1(r) \to R_\infty$ and Eq. (13) give an effective source with the asymptotic form $\rho_{\rm eff} \propto r^{-2}$. In the weak-field limit the gravitational acceleration is determined by the enclosed effective mass through

$$g(r) = \frac{G M_{\rm eff}(r)}{r^2}. \tag{20}$$

Importantly, this contribution is not merely kinematic: it enters the gravitational field equations through Eq. (11). If $\rho_{\rm eff} \propto r^{-2}$, the enclosed mass grows linearly with radius

$$M_{\rm eff}(r) \propto r, \tag{21}$$

which leads to an asymptotic acceleration

$$g_h(r) \propto \frac{1}{r}. \tag{22}$$

The circular velocity then follows from the standard relation

$$v^2(r) = r\, g(r), \tag{23}$$

yielding an approximately constant asymptotic velocity

$$v(r) \to v_f = \text{const.} \tag{24}$$

The required source scale can be written directly. For a flat rotation curve with velocity v_f, Eq. (20) gives

$$\rho_{\rm eff}(r) = \frac{v_f^2}{4\pi G r^2}. \tag{25}$$

Equivalently, the active energy density required from the rotational stress sector is $c^2\rho_{\rm eff}$. For $v_f \sim 2 \times 10^5\,\mathrm{m\,s^{-1}}$ and $r = 10\,\mathrm{kpc}$, Eq. (25) gives

$$\rho_{\rm eff} \sim 5 \times 10^{-22}\,\mathrm{kg\,m^{-3}} \simeq 7 \times 10^{-3}\,M_\odot\,\mathrm{pc^{-3}}. \tag{26}$$

This scale is galactic and macroscopic. It is not the scale of an ordinary post-Newtonian frame-dragging correction. Therefore the viability condition is that the Alena Tensor rotational sector contributes to the active source in Eq. (11) with the magnitude specified by Eq. (25).

Matching the asymptotic velocity with the baryonic Tully-Fisher relation imposes the scaling

$$v_f^4 \propto R_\infty. \tag{27}$$

Within this framework, Eq. (27) is a consistency condition on the asymptotic transport amplitude rather than a first-principles derivation of the baryonic Tully-Fisher relation. Equivalently, using Eq. (19), the

 doi:10.20944/preprints202603.1718.v2

corresponding asymptotic angular-momentum transport rate is macroscopically large, as expected for a collective galactic-scale stress channel. The empirical BTFR then requires the dominant transport mode to scale with the baryonic mass of the system,

$$R_\infty \propto M_b. \tag{28}$$

A minimal radial profile satisfying both Eq. (14) and the asymptotic scaling can therefore be written as

$$R_1(r) = R_\infty \frac{r^n}{r^n + r_c^n}, \quad n > 2, \tag{29}$$

where r_c defines the transition scale between the baryon-dominated inner region and the rotationally supported halo regime.

5. Predictions

The mechanism discussed above leads to a set of observational and theoretical predictions that can be compared with both dark matter and modified-gravity scenarios. The principal testable consequences are summarised below.

5.1. Anisotropic Gravitational Lensing Aligned with the Baryonic Disk

The dominant $\ell = 1$ Legendre mode of the stream potential Ψ produces an effective density distribution that is flattened and co-aligned with the baryonic disk. This geometry differs from the approximately spherical idealization often used for NFW halos in ΛCDM and from the isotropic phantom dark matter profile of isolated MOND/TeVeS systems. It therefore gives a testable prediction for the azimuthal dependence of the weak-lensing shear signal around disk galaxies.

In ΛCDM, halo triaxiality can produce an anisotropic shear signal, although the signal is affected by baryonic alignment, projection, and the radial structure of the halo. A 3.8σ detection of halo ellipticity aligned with galaxy light has already been obtained from stacked galaxy-galaxy lensing [16]. In MOND/TeVeS, the lensing signal away from an isolated lens is expected to be closer to isotropic in the absence of an external-field or environmental contribution [17]. In the present mechanism the effective matter distribution is disk-aligned and flattened, so the anisotropic shear signal should scale with disk inclination angle i as $\Delta\gamma \propto \sin^2 i$ at fixed M_b.

The inclination dependence of disk galaxy lensing has recently been analysed in the MOND framework by Harvey-Hawes & Galoppo [18], who show that inclination effects on the strong-lensing cross section are enhanced relative to ΛCDM precisely because no spherical halo suppresses the disk geometry. In the present mechanism an analogous but distinct signature is predicted in the weak-lensing regime: the quadrupole moment of the stacked shear field, measured as a function of i, should follow the disk-plane geometry of the transport mode rather than the stellar light distribution used as a proxy in current analyses [16]. A detection of a positive $\Delta\gamma - \sin^2 i$ correlation at fixed M_b in forthcoming Euclid or LSST weak-lensing catalogues, with the signal following the disk-plane geometry of the transport mode, would provide a direct observational test of the transport-driven origin of the effective halo.

5.2. Disk-State Dependence of Halo Scaling at High Redshift

In the present framework R_∞ builds up on the local orbital timescale $\tau_J \sim R_d/v_f$ as the disk establishes a quasi-stationary angular-momentum transport channel. The discriminating prediction is therefore not a shift in the mean BTFR at high z, but a specific structure of its residuals: galaxies in a dynamically immature state ($V/\sigma \lesssim 3$, disturbed morphology, young mean stellar age) should lie below the BTFR at fixed M_b, while dynamically settled disks should recover the local relation at any epoch, consistent with JWST detections of massive cold disks at $z \gtrsim 4-6$ [19,20] and with the absence of significant BTFR evolution to $z \sim 2.5$ [21].

 doi:10.20944/preprints202603.1718.v2

Quantitatively, the BTFR residual at fixed M_b is predicted to satisfy

$$\delta \log v_f \;\propto\; -f\!\left(\frac{t_{\rm age}}{\tau_J}\right), \quad f(x) \xrightarrow{x\to\infty} 0, \quad f(x) \approx e^{-x} \tag{30}$$

at leading order, so that the residual decays with dynamical age and vanishes for relaxed systems. A partial correlation between $\delta \log v_f$ and V/σ at fixed M_b, with the sign specified by Eq. (30), is testable with JWST NIRSpec IFU samples at $z > 4$. This correlation is not a generic MOND prediction, where a_0 carries no disk-state dependence, and would differ from the usual ΛCDM interpretation in which BTFR residuals are mainly tied to halo concentration, feedback, and assembly history.

5.3. Suppressed Halo Scaling in Low-Angular-Momentum Systems: Connection to Ultra-Diffuse Galaxies

Since $R_\infty \propto M_b$ and the transport amplitude is set by the baryonic angular-momentum budget, systems with intrinsically low specific angular momentum $j_b \equiv J_b/M_b$ are predicted to have anomalously small R_∞, producing rotation curves consistent with the baryonic contribution alone and no effective halo enhancement. Ultra-diffuse galaxies (UDGs) with suppressed or absent halo-like scaling, such as NGC 1052-DF2 and NGC 1052-DF4 [22,23], and the recently identified FCC 224 [24] are natural candidates for this low-j_b tail. In this interpretation the wide dispersion in halo-like amplitude across the UDG population is expected to reflect the dispersion in j_b at fixed M_b.

A critical distinction from the standard ΛCDM high-spin scenario arises here. Cosmological simulations associate extended UDG morphologies with high halo spin λ [25], yet recent EAGLE results show that UDG sizes are driven not by high halo spin but by high spin in the star-forming gas [26], with angular momentum acquired through circumgalactic interactions. In the present framework the relevant quantity is j_b of the baryonic disk rather than the total halo spin, so UDGs formed via tidal stripping or feedback-driven gas expulsion (processes that reduce j_b without necessarily lowering λ) are predicted to fall below the effective halo scaling relation at fixed M_b.

A testable corollary follows: within a sample of UDGs at fixed stellar mass, the kinematic proxy λ_R measured by integral-field spectroscopy [27] should correlate positively with the amplitude of the halo-like velocity excess above the baryonic prediction. The two kinematic classes of UDGs identified by MUSE observations, rotation-supported versus dispersion-dominated [24], provide an existing dataset to test this prediction, with rotation-supported UDGs expected to lie on the standard scaling relation and dispersion-dominated ones to fall systematically below it.

5.4. Geometry-Locked Transition Radii and Systematic RAR Residuals

In the present framework the transition radius r_c is not a free parameter but is set by the geometry of the baryonic disk, since higher Legendre modes of the stream potential decay faster with radius and may resonate with structural scales such as the disk scale radius R_d, the bar corotation radius, or the stellar-to-gas transition scale. This leads to the prediction that r_c is not distributed randomly across the galaxy population but clusters near integer multiples of characteristic disk scales, producing a systematic correlation between the location of the baryonic-to-rotational transition and disk structural parameters.

Current data from SPARC already constrain this picture tightly. The RAR shows an observed scatter of only $\sim$ 0.057 dex after fitting 175 individual galaxies [28], with no strong evidence for significant galaxy-to-galaxy variation in the critical acceleration scale [28,29]. Within the present framework this tight universality is natural if r_c scales proportionally with R_d, so that the transition always occurs at a fixed fraction of the disk scale, preserving the mean RAR shape while allowing residuals correlated with $R_d/R_{\rm eff}$. Non-monotonic features (upward or downward hooks in the $[g_{\rm bar}, g_{\rm obs}]$ plane) observed in resolved kinematic data of individual galaxies [30] are a direct signature of a locally non-trivial $R_1(r)$ profile, consistent with the mode structure of (8) for $n > 2$.

The discriminating prediction of the present mechanism is therefore a partial correlation between RAR residuals and disk structural parameters, specifically, $\delta g_{\rm obs}$ at fixed $g_{\rm bar}$ should correlate with

 doi:10.20944/preprints202603.1718.v2

R_d and with the bar-to-disk mass ratio at constant M_b. This correlation is not expected in a strictly universal MOND interpolation function depending only on $|g_{\rm bar}|/a_0$ [28,29], and differs from the usual ΛCDM expectation in which RAR residuals are primarily associated with halo concentration, feedback, and assembly history rather than directly with disk geometry. A complementary test is provided by the RAR on cluster scales, where the effective acceleration scale is found to be ~ 17 times larger than for disk galaxies [31–33]: in the present framework this elevation reflects the absence of an efficient baryonic angular-momentum transport channel on cluster scales, where the baryonic component does not form a coherent rotating disk, and $R_\infty \to 0$.

5.5. Baryonic Specific Angular Momentum as the Primary Secondary Parameter of Halo Scaling

In the present mechanism the effective halo amplitude is controlled by the asymptotic baryonic angular-momentum transport rate $\dot{J}_\infty \propto M_b v_f^2$, so the relevant secondary parameter at fixed M_b is the baryonic specific angular momentum $j_b \equiv J_b/M_b$, not the dark matter halo spin λ. This distinction is observationally sharp: IllustrisTNG and EAGLE simulations find negligible correlation between the stellar disc spin and the host halo spin [34,35], with a mean angular-momentum retention factor $f_j \approx 0.5$ [34], so that j_b and λ are effectively decoupled at the disc scale.

Current data already constrain this prediction non-trivially. The BTFR shows no strong correlation between its residuals and any galaxy structural parameter at fixed M_b [28,36,37], which is consistent with the present framework only if j_b itself is nearly independent of M_b at fixed V_f, a condition satisfied by the observed tight power-law $j_b \propto M_b^{0.60}$ [38]. At the same time, the Fall relation (j_b vs. M_b) carries $\sim 7\times$ more scatter than the BTFR [28,36], with residuals driven by the gas fraction: at fixed M_b, gas-poor galaxies have systematically lower j_b [38]. In the present framework this translates directly into a prediction: gas-poor galaxies at fixed M_b should exhibit weaker halo-like velocity enhancement, i.e. negative BTFR residuals correlated with low $f_{\rm gas}$.

This prediction is testable with the SPARC sample augmented by gas-fraction measurements. A partial correlation

$$\delta \log V_f\Big|_{M_b} \propto +\alpha\, \delta \log j_b\Big|_{M_b}, \quad \alpha > 0, \tag{31}$$

with α set by the transport efficiency, should be present in the data at the level of the Fall-relation scatter. In the usual ΛCDM interpretation, BTFR residuals are attributed primarily to halo concentration variations [39], which correlate with assembly history rather than directly with $f_{\rm gas}$ or j_b at fixed M_b. In MOND, no such secondary dependence follows from a universal a_0. A detection of the $\delta \log V_f - f_{\rm gas}$ correlation at fixed M_b in the SPARC or MHONGOOSE samples, with the sign specified by (31), would therefore favour the transport-driven origin of halo scaling.

6. Consistency with Existing Observations

Mentioned predictions can be confronted with data already available in the literature, allowing for non-trivial consistency checks without introducing additional free parameters or performing new rotation-curve fits.

6.1. Elevated Acceleration Scale in Galaxy Clusters

The radial acceleration relation (RAR) established for late-type disk galaxies [28,29] exhibits a characteristic acceleration scale $g_\dagger \approx 1.2 \times 10^{-10}\,\mathrm{m\,s^{-2}}$. On brightest-cluster-galaxy (BCG) and cluster scales, however, the effective acceleration scale is elevated by a factor of approximately seventeen [31–33], a discrepancy as indicated by studies combining kinematics, gravitational lensing, and X-ray thermodynamic mass profiles [40]. This scale-dependent behaviour is in tension with a strictly universal MOND acceleration scale and provides a non-trivial comparison point for ΛCDM cluster modelling.

Within the present framework this difference arises naturally from the absence of a coherent rotating baryonic disk on cluster scales. The baryonic component of clusters is dominated by a hot, quasi-isotropic intracluster medium, so the angular-momentum transport channel discussed above

 doi:10.20944/preprints202603.1718.v2

is not efficiently established. As a result the effective contribution associated with the transport mode is strongly suppressed, and the observed acceleration reflects predominantly the baryonic mass distribution. The observed elevation of the effective acceleration scale is therefore consistent with the predicted dependence on the degree of rotational organisation of the baryonic component.

6.2. Ultra-Diffuse Galaxies with Suppressed Halo Scaling

A second class of systems providing an existing consistency check are ultra-diffuse galaxies (UDGs) with anomalously low or absent halo-like velocity enhancements. NGC 1052-DF2 was the first confirmed example of a galaxy whose stellar velocity dispersion is consistent with its baryonic mass alone [23], followed by NGC 1052-DF4 [41] and, more recently, NGC 1052-DF9, whose kinematics are likewise inconsistent with a standard dark matter halo at high significance [42].

These objects are plausibly associated with a dynamical formation channel involving strong interactions or collisions that disrupt any pre-existing disk structure [43]. In such systems the lack of a coherent baryonic disk implies that the angular-momentum transport mechanism is not sustained, so the additional halo-like contribution is expected to be suppressed. The observed kinematics are therefore consistent with the expectation that systems with suppressed or disrupted baryonic angular momentum exhibit reduced or absent effective halo scaling.

An analogous case, FCC 224 in the Fornax cluster [24], indicates that such systems are not unique to a single environment. Moreover, the observed division of UDGs into rotation-supported and dispersion-dominated subclasses [24] is qualitatively consistent with the dependence on dynamical state: systems retaining coherent rotation tend to exhibit higher velocity support than dispersion-dominated counterparts at comparable stellar mass.

6.3. Anisotropic Weak-Lensing Signal Aligned with the Baryonic Disk

Weak-lensing measurements of galaxy-scale mass distributions provide an additional empirical point of contact. Stacked galaxy-galaxy lensing analyses have reported non-zero halo ellipticity aligned with the stellar light distribution [17,44], with subsequent studies confirming this trend for specific galaxy populations.

This observational result is qualitatively consistent with a flattened, disk-aligned effective matter distribution, as expected if the dominant contribution is tied to the baryonic geometry rather than to an underlying spherical halo. While current measurements typically use stellar light as a proxy for orientation, and therefore do not directly isolate the geometric dependence discussed above, the presence of a statistically significant anisotropic signal is consistent with a disk-aligned effective source and motivates more direct inclination-dependent tests.

Future surveys will be required to test the more specific inclination-dependent scaling predicted in the previous section, however, existing detections of aligned ellipticity provide an important consistency check of the basic geometric picture.

7. Discussion

The analysis presented here provides a framework in which halo-like phenomenology of galaxies arises from the rotational sector of the matter energy-momentum tensor, rather than from additional dark matter particles or modifications of gravity. In this picture the effective halo contribution originates from angular-momentum transport encoded in the mixed stress-energy components $T^r{}_\phi$ and $T^\theta{}_\phi$, and the resulting effective density distribution is generically anisotropic. In particular, the dominant transport mode produces flattened, disk-aligned halo structures rather than spherical halos. This differs from approximately spherical halo idealizations and from MOND-like descriptions in which the isolated effective modification is isotropic. The framework therefore leads to inclination-dependent gravitational effects, including anisotropic lensing signatures. Existing weak-lensing measurements indicating non-zero halo ellipticity aligned with galaxy light are qualitatively consistent with this picture, although more discriminating tests are required.

 doi:10.20944/preprints202603.1718.v2

The conservation of the corresponding Killing current naturally introduces a stream potential describing the transport of angular momentum in the meridional plane. Its angular structure is governed by Legendre modes, with the lowest odd multipole $\ell = 1$ dominating the radial flux on the galactic plane. Together with the active-source closure in Eq. (12), this leads to an r^{-2} scaling of the effective halo contribution in the weak-field regime. The observational scaling relations further restrict the class of admissible solutions. The RAR requires that the rotational sector vanishes sufficiently rapidly toward the galactic centre, while the baryonic Tully-Fisher relation constrains the asymptotic amplitude of the dominant Legendre mode through the baryonic mass of the system. These constraints leave a narrow class of radial profiles characterized by a transition scale separating the baryonic and rotational regimes. The observed tightness and apparent universality of these relations are consistent with a mechanism governed primarily by baryonic properties rather than by stochastic halo assembly.

In this interpretation galactic halos correspond to macroscopic transport modes of angular momentum generated by rotational stresses in relativistic matter. The observed halo phenomenology may therefore reflect large-scale collective behaviour encoded in the structure of the energy-momentum tensor itself. This interpretation is consistent with systems in which the transport channel is expected to be inefficient: galaxy clusters, which lack coherent rotation, and ultra-diffuse galaxies with disrupted or low-angular-momentum disks both exhibit suppressed or altered halo-like scaling consistent with this expectation. This picture is consistent with the broader astrophysical context in which correlated stresses and torques transport angular momentum outwards in rotating systems [15,45]. The efficiency of the transport channel could plausibly arise from correlated gravitational torques and vortical stresses in the disk-halo system, analogous to angular momentum transport mechanisms discussed in galactic disk dynamics. In the present framework, the same transport channel contributes to the gravitational source term, so the halo can be interpreted as a gravitating collective rotational mode of matter.

The present framework also suggests a dynamical route toward the scaling entering the baryonic Tully-Fisher relation. As shown, the asymptotic amplitude R_∞ is directly related to the radial angular-momentum current carried by the rotational sector, implying $v_f^4 \propto R_\infty \propto \dot{J}_\infty$. If the outward transport of angular momentum operates on a timescale comparable to the orbital timescale of the baryonic disk $\tau_J \sim R_d/v_f$ [46], then $\dot{J}_\infty \sim J_b/\tau_J$, where J_b is the total baryonic angular momentum. Using $J_b \sim M_b R_d v_f$ for rotationally supported disks then gives $\dot{J}_\infty \sim M_b v_f^2$. Since the halo amplitude is controlled by R_∞, this scaling gives the condition required by the baryonic Tully-Fisher relation. In this interpretation the BTFR reflects the efficiency of large-scale angular-momentum redistribution in the baryonic disk. Deviations from the ideal relation are expected to trace variations in transport efficiency and baryonic angular momentum, providing a direct observational handle on the mechanism. A quantitative derivation requires a full dynamical model of angular-momentum transport and is left for future work.

8. Limitations and Future Work

The existence of a finite asymptotic transport amplitude is interpreted here as the large-radius outcome of sustained angular-momentum redistribution in rotating systems. The present analysis, however, remains limited to the weak-field regime and does not provide a full dynamical solution for R_∞. A complete treatment requires the coupled evolution of the metric, vorticity, shear, energy flux, and anisotropic stress in Eq. (2).

The central theoretical task is the first-principles normalization of the closure in Eq. (12). The existence of large-scale angular-momentum transport is not an additional assumption; it is a standard feature of rotating astrophysical systems and is supported by the transport regimes discussed above. What remains specific to the present framework is the Alena Tensor identification of this rotational transport sector with an active weak-field source of the magnitude required by Eq. (25). If the rotational sector generated only the ordinary post-Newtonian gravitomagnetic correction, the effect would be too small for galactic rotation curves. The mechanism is viable when the Alena Tensor stress sector

 doi:10.20944/preprints202603.1718.v2

contributes to the active source in Eq. (11) at the macroscopic scale specified by Eq. (25). This condition must be tested against stability, lensing, disk dynamics, and energy-condition constraints.

Future work should therefore determine $R_1(r)$ from the full transport equations, calculate the normalization of Eq. (12), and perform joint fits to rotation curves and lensing data. The observational predictions listed above provide direct tests: disk-aligned lensing anisotropy, residual dependence on baryonic angular momentum, and suppression in systems without coherent rotation.

In summary, the rotational sector of the energy-momentum tensor provides a testable framework for describing halo-like phenomenology within standard gravity. Its key predictions: anisotropic effective density distributions, dependence on baryonic angular momentum, and suppression in systems without coherent rotation are already in qualitative agreement with several classes of observations and can be tested more stringently with forthcoming data [47,48].

9. Statements

All data that support the findings of this study are included within the article (and any supplementary files).

During the preparation of this work the author did not use generative AI or AI-assisted technologies, except for continuous learning.

Author did not receive support from any organization for the submitted work.

Author have no relevant financial or non-financial interests to disclose.

References

1. Ruan, D.; Brooks, A.M.; Cruz, A.; Peter, A.H.; Keller, B.W.; Quinn, T.; Wadsley, J.; Adams, E.A. Predictions for detecting a turndown in the baryonic Tully–Fisher relation. *Monthly Notices of the Royal Astronomical Society* **2025**, *541*, 2180–2196. https://doi.org/10.1093/mnras/staf1099.
2. Kourkchi, E.; Tully, R.B.; Courtois, H.M.; Dupuy, A.; Guinet, D. Cosmicflows-4: the baryonic Tully–Fisher relation providing 10 000 distances. *Monthly Notices of the Royal Astronomical Society* **2022**, *511*, 6160–6178. https://doi.org/10.1093/mnras/stac303.
3. Salucci, P. Issues in the Investigations of the Dark Matter Phenomenon in Galaxies: Parcere Personis, Dicere de Vitiis. *Universe* **2025**, *11*, 67. https://doi.org/10.3390/universe11020067.
4. Abdalla, E.; Marins, A. The dark sector cosmology. *International Journal of Modern Physics D* **2020**, *29*, 2030014. https://doi.org/10.1142/S0218271820300141.
5. Zhai, Y.; De Cesare, M.; Van De Bruck, C.; Di Valentino, E.; Wilson-Ewing, E. A low-redshift preference for an interacting dark energy model. *Journal of Cosmology and Astroparticle Physics* **2025**, *2025*, 010. https://doi.org/10.1088/1475-7516/2025/11/010.
6. Ogonowski, P. The halo effect and quantum vortices. Not so dark with Alena Tensor. *Physica Scripta* **2026**, *101*, 155002. https://doi.org/10.1088/1402-4896/ae59ca.
7. Eappen, R.; Kroupa, P. Scaling relations of early-type galaxies in MOND. *Galaxies* **2025**, *13*, 22. https://doi.org/10.3390/galaxies13020022.
8. Domènech, G.; Ganz, A. Connecting relativistic MOND theories with mimetic gravity. *Journal of Cosmology and Astroparticle Physics* **2025**, *2025*, 059. https://doi.org/10.1088/1475-7516/2025/06/059.
9. Yoo, J.; Magi, M.; Huterer, D. Cosmic dipoles from large-scale structure surveys. *Phys. Rev. D* **2025**, *112*, 123013. https://doi.org/10.1103/ks44-qt3b.
10. Kratter, K.; Lodato, G. Gravitational instabilities in circumstellar disks. *Annual Review of Astronomy and Astrophysics* **2016**, *54*, 271–311. https://doi.org/10.1146/annurev-astro-081915-023307.
11. Cesare, V. Dark coincidences: Small-scale solutions with refracted gravity and mond. *Universe* **2023**, *9*, 56. https://doi.org/10.3390/universe9010056.
12. Hopkins, P.F.; Quataert, E. An analytic model of angular momentum transport by gravitational torques: from galaxies to massive black holes. *Monthly Notices of the Royal Astronomical Society* **2011**, *415*, 1027–1050. https://doi.org/10.1111/j.1365-2966.2011.18542.x.
13. Krumholz, M.R.; Burkhart, B.; Forbes, J.C.; Crocker, R.M. A unified model for galactic discs: star formation, turbulence driving, and mass transport. *Monthly Notices of the Royal Astronomical Society* **2018**, *477*, 2716–2740. https://doi.org/10.1093/mnras/sty852.

 doi:10.20944/preprints202603.1718.v2

14. Yang, H.; Liao, S.; Fattahi, A.; Frenk, C.S.; Gao, L.; Guo, Q.; Shao, S.; Wang, L.; Wright, R.J.; Zeng, G. APOSTLE–AURIGA: effects of stellar feedback subgrid models on the evolution of angular momentum in disc galaxies. *Monthly Notices of the Royal Astronomical Society* **2024**, *535*, 1394–1405. https://doi.org/10.1093/mnras/stae2411.
15. Trapp, C.W.; Kereš, D.; Hopkins, P.F.; Faucher-Giguère, C.A.; Murray, N. Angular momentum transfer in cosmological simulations of Milky Way-mass discs. *Monthly Notices of the Royal Astronomical Society* **2024**, *533*, 3008–3026. https://doi.org/10.1093/mnras/stae2021.
16. Bacon, D.J.; Refregier, A.R.; Ellis, R.S. Detection of weak gravitational lensing by large-scale structure. *Monthly Notices of the Royal Astronomical Society* **2000**, *318*, 625–640. https://doi.org/10.1046/j.1365-8711.2000.03851.x.
17. Hoekstra, H.; Yee, H.K.; Gladders, M.D. Properties of galaxy dark matter halos from weak lensing. *The Astrophysical Journal* **2004**, *606*, 67–77. https://doi.org/10.1086/382726.
18. Harvey-Hawes, C.; Galoppo, M. A Novel Test for MOND: Gravitational Lensing by Disk Galaxies. *The Astrophysical Journal* **2025**, *994*, 167. https://doi.org/10.3847/1538-4357/ae11ad.
19. Rizzo, F.; Vegetti, S.; Powell, D.; Fraternali, F.; McKean, J.; Stacey, H.; White, S. A dynamically cold disk galaxy in the early Universe. *Nature* **2020**, *584*, 201–204. https://doi.org/10.1038/s41586-020-2572-6.
20. Wang, W.; Cantalupo, S.; Pensabene, A.; Galbiati, M.; Travascio, A.; Steidel, C.C.; Maseda, M.V.; Pezzulli, G.; De Beer, S.; Fossati, M.; et al. A giant disk galaxy two billion years after the Big Bang. *Nature Astronomy* **2025**, *9*, 710–719. https://doi.org/10.1038/s41550-025-02500-2.
21. Übler, H.D.; Genzel, R.; Wisnioski, E.; Schreiber, N.M.F.; Shimizu, T.T.; Price, S.H.; Tacconi, L.J.; Belli, S.; Wilman, D.J.; Fossati, M.; et al. The Evolution and Origin of Ionized Gas Velocity Dispersion from $z \sim 2.6$ to $z \sim 0.6$ with KMOS^{3D}. *arXiv preprint arXiv:1906.02737* **2019**. https://doi.org/10.3847/1538-4357/ab27cc.
22. Van Dokkum, P.; Danieli, S.; Cohen, Y.; Merritt, A.; Romanowsky, A.J.; Abraham, R.; Brodie, J.; Conroy, C.; Lokhorst, D.; Mowla, L.; et al. A galaxy lacking dark matter. *Nature* **2018**, *555*, 629–632. https://doi.org/10.1038/nature25767.
23. Danieli, S.; van Dokkum, P.; Conroy, C.; Abraham, R.; Romanowsky, A.J. Still missing dark matter: KCWI high-resolution stellar kinematics of NGC1052-DF2. *The Astrophysical Journal Letters* **2019**, *874*, L12. https://doi.org/10.3847/2041-8213/ab0e8c.
24. Buzzo, M.L.; Forbes, D.A.; Romanowsky, A.J.; Haacke, L.; Gannon, J.S.; Tang, Y.; Hilker, M.; Ferré-Mateu, A.; Janssens, S.R.; Brodie, J.P.; et al. A new class of dark matter-free dwarf galaxies?-I. Clues from FCC 224, NGC 1052-DF2, and NGC 1052-DF4. *Astronomy & Astrophysics* **2025**, *695*, A124. https://doi.org/10.1051/0004-6361/202453522.
25. Benavides, J.A.; Sales, L.V.; Abadi, M.G.; Marinacci, F.; Vogelsberger, M.; Hernquist, L. Origin and evolution of ultradiffuse galaxies in different environments. *Monthly Notices of the Royal Astronomical Society* **2023**, *522*, 1033–1048. https://doi.org/10.1093/mnras/stad1053.
26. Zheng, H.; Liao, S.; Gao, L.; Jiang, F. Ultradiffuse Galaxies in the EAGLE Simulation. *The Astrophysical Journal* **2026**, *997*, 15. https://doi.org/10.3847/1538-4357/ae260f.
27. Buttitta, C.; Iodice, E.; Doll, G.; Hartke, J.; Hilker, M.; Forbes, D.A.; Corsini, E.M.; Rossi, L.; Arnaboldi, M.; Cantiello, M.; et al. Looking into the faintEst WIth MUSE (LEWIS): Exploring the nature of ultra-diffuse galaxies in the Hydra-I cluster-II. Stellar kinematics and dynamical masses. *Astronomy & Astrophysics* **2025**, *694*, A276. https://doi.org/10.1051/0004-6361/202452915.
28. Lelli, F.; McGaugh, S.S.; Schombert, J.M.; Pawlowski, M.S. One law to rule them all: the radial acceleration relation of galaxies. *The Astrophysical Journal* **2017**, *836*, 152. https://doi.org/10.3847/1538-4357/836/2/152.
29. Li, P.; Lelli, F.; McGaugh, S.; Schombert, J. Fitting the radial acceleration relation to individual SPARC galaxies. *Astronomy & Astrophysics* **2018**, *615*, A3. https://doi.org/10.1051/0004-6361/201732547.
30. Mercado, F.J.; Bullock, J.S.; Moreno, J.; Boylan-Kolchin, M.; Hopkins, P.F.; Wetzel, A.; Faucher-Giguère, C.A.; Samuel, J. Hooks & Bends in the radial acceleration relation: discriminatory tests for dark matter and MOND. *Monthly Notices of the Royal Astronomical Society* **2024**, *530*, 1349–1362. https://doi.org/10.1093/mnras/stae819.
31. Tian, Y.; Ko, C.M.; Li, P.; McGaugh, S.; Poblete, S.L. A distinct radial acceleration relation across the brightest cluster galaxies and galaxy clusters. *Astronomy & Astrophysics* **2024**, *684*, A180. https://doi.org/10.1051/0004-6361/202347868.
32. Allen, S.W.; Evrard, A.E.; Mantz, A.B. Cosmological parameters from observations of galaxy clusters. *Annual Review of Astronomy and Astrophysics* **2011**, *49*, 409–470. https://doi.org/10.1146/annurev-astro-081710-102514.

 doi:10.20944/preprints202603.1718.v2

33. Umetsu, K. Cluster–galaxy weak lensing: K. Umetsu. *The Astronomy and Astrophysics Review* **2020**, *28*, 7. https://doi.org/10.1007/s00159-020-00129-w.
34. Zjupa, J.; Springel, V. Angular momentum properties of haloes and their baryon content in the Illustris simulation. *Monthly Notices of the Royal Astronomical Society* **2017**, *466*, 1625–1647. https://doi.org/10.1093/mnras/stw2945.
35. Yang, H.; Gao, L.; Frenk, C.S.; Grand, R.J.; Guo, Q.; Liao, S.; Shao, S. The galaxy size to halo spin relation of disc galaxies in cosmological hydrodynamical simulations. *Monthly Notices of the Royal Astronomical Society* **2023**, *518*, 5253–5259. https://doi.org/10.1093/mnras/stac3335.
36. Lelli, F.; McGaugh, S.S.; Schombert, J.M.; Desmond, H.; Katz, H. The baryonic Tully-Fisher relation for different velocity definitions and implications for galaxy angular momentum. *Monthly Notices of the Royal Astronomical Society* **2019**, *484*, 3267–3278. https://doi.org/10.1093/mnras/stz205.
37. McGaugh, S.S.; Schombert, J.M.; Bothun, G.D.; De Blok, W. The baryonic tully-fisher relation. *The Astrophysical Journal Letters* **2000**, *533*, L99–L102. https://doi.org/10.1086/312628.
38. Piña, P.E.M.; Posti, L.; Fraternali, F.; Adams, E.A.; Oosterloo, T. The baryonic specific angular momentum of disc galaxies. *Astronomy & Astrophysics* **2021**, *647*, A76. https://doi.org/10.1051/0004-6361/202039340.
39. Desmond, H.; Wechsler, R.H. The Tully–Fisher and mass–size relations from halo abundance matching. *Monthly Notices of the Royal Astronomical Society* **2015**, *454*, 322–343. https://doi.org/10.1093/mnras/stv1978.
40. Li, P.; Tian, Y.; Júlio, M.P.; Pawlowski, M.S.; Lelli, F.; McGaugh, S.S.; Schombert, J.M.; Read, J.I.; Yu, P.C.; Ko, C.M. Measuring galaxy cluster mass profiles into the low-acceleration regime with galaxy kinematics. *Astronomy & Astrophysics* **2023**, *677*, A24. https://doi.org/10.1051/0004-6361/202346431.
41. van Dokkum, P.; Danieli, S.; Abraham, R.; Conroy, C.; Romanowsky, A.J. A second galaxy missing dark matter in the NGC 1052 group. *The Astrophysical Journal Letters* **2019**, *874*, L5. https://doi.org/10.3847/2041-8213/ab0d92.
42. Keim, M.A.; van Dokkum, P.; Shen, Z.; Danieli, S.; Pasha, I. A Third Galaxy Missing Dark Matter along a Trail of Galaxies in the NGC 1052 Field. *arXiv preprint arXiv:2603.15860* **2026**. https://doi.org/10.48550/arXiv.2603.15860.
43. van Dokkum, P.; Shen, Z.; Keim, M.A.; Trujillo-Gomez, S.; Danieli, S.; Dutta Chowdhury, D.; Abraham, R.; Conroy, C.; Kruijssen, J.D.; Nagai, D.; et al. A trail of dark-matter-free galaxies from a bullet-dwarf collision. *Nature* **2022**, *605*, 435–439. https://doi.org/10.1038/s41586-022-04665-6.
44. Mandelbaum, R.; Hirata, C.M.; Broderick, T.; Seljak, U.; Brinkmann, J. Ellipticity of dark matter haloes with galaxy–galaxy weak lensing. *Monthly Notices of the Royal Astronomical Society* **2006**, *370*, 1008–1024. https://doi.org/10.1111/j.1365-2966.2006.10539.x.
45. Sellwood, J. The lifetimes of spiral patterns in disc galaxies. *Monthly Notices of the Royal Astronomical Society* **2011**, *410*, 1637–1646. https://doi.org/10.1111/j.1365-2966.2010.17545.x.
46. Hafen, Z.; Stern, J.; Bullock, J.S.; Gurvich, A.B.; Yu, S.; Faucher-Giguère, C.A.; Fielding, D.B.; Anglés-Alcázar, D.; Quataert, E.; Wetzel, A.; et al. Hot-mode accretion and the physics of thin-disc galaxy formation. *Monthly Notices of the Royal Astronomical Society* **2022**, *514*, 5056–5073. https://doi.org/10.1093/mnras/stac1603.
47. Becattini, F.; Singh, R. On the local thermodynamic relations in relativistic spin hydrodynamics. *The European Physical Journal C* **2025**, *85*, 1338. https://doi.org/10.1140/epjc/s10052-025-15071-3.
48. Kiamari, M.; Sadooghi, N.; Sedighi Jafari, M. Relativistic magnetohydrodynamics of a spinful and vortical fluid: Entropy current analysis. *Physical Review D* **2024**, *109*, 036024. https://doi.org/10.1103/PhysRevD.109.036024.